PHYSICAL REVIEW A VOLUME 54, NUMBER 1 JULY 1996

Diffusion of barium atoms in the $6s5d\ ^3D_J$ metastable levels and the $6s^2\ ^1S_0$ ground state through noble-gas perturbers

R. K. Namiotka, E. Ehrlacher,* J. Sagle, M. Brewer,† D. J. Namiotka,‡ A. P. Hickman, A. D. Streater, and J. Huennekens
Department of Physics, Lehigh University, 16 Memorial Drive East, Bethlehem, Pennsylvania 18015

(Received 10 January 1996; revised manuscript received 29 March 1996)

We describe a set of experiments that investigate diffusion of barium $6s5d\ ^3D_J$ metastable level and $6s^2\ ^1S_0$ ground-state atoms through the noble gases: He, Ne, Ar, Kr, and Xe. The barium metastable levels were populated through optical pumping of the $6s^2\ ^1S_0 \rightarrow 6s6p\ ^3P_1^o$ intercombination transition with a pulsed laser, followed by spontaneous or stimulated emission into the $6s5d\ ^3D_{1,2}$ levels. Collisional mixing then distributed population throughout the $6s5d\ ^3D_J$ levels. A weak narrow-band cw laser was tuned to appropriate transitions to probe the spatial distribution of metastable level atoms, as well as the hole created in the ground-state spatial distribution, by the pulsed laser. Time-dependent absorption coefficients were obtained by measuring the transmission of the probe laser at several different pump-probe spatial separations. From these absorption data, spatial number density profiles were mapped out for various times following the firing of the pump laser. These density profiles were used to determine the diffusion coefficient for each state at a particular buffer-gas pressure and temperature. From these pressure- and temperature-dependent diffusion coefficients D, we determined the thermally averaged diffusion cross sections $\sigma_D(6s5d\ ^3D_J)$ and $\sigma_D(6s^2\ ^1S_0)$ for the metastable and ground-state atoms diffusing through the noble gases, respectively. We also report values for the scaled standard diffusion coefficients D_0. Our experimental values of the thermally averaged diffusion cross sections $\sigma_D(6s5d\ ^3D_J)$ and $\sigma_D(6s^2\ ^1S_0)$ for the barium-helium system are compared with values calculated from published, theoretical barium-helium potentials and the agreement is excellent. [S1050-2947(96)07706-2]

PACS number(s): 34.20.Cf, 51.20.+d

I. INTRODUCTION

We describe a set of experiments in which we measure the thermally averaged velocity-changing collision (diffusion) cross sections σ_D for barium ($6s5d\ ^3D_J$) and barium ($6s^2\ ^1S_0$)–noble-gas collisions. The measurements are made using a pulsed-pump–cw-probe technique, which allows us to follow the evolution of the spatial distribution of atoms in time. The pulsed laser pumps the barium $6s^2\ ^1S_0 \rightarrow 6s6p\ ^3P_1^o$ transition. Excited atoms then radiate back to the ground state or down to the $6s5d\ ^3D_J$ levels. Once in the $6s5d\ ^3D_J$ states, the atoms are essentially trapped (see Fig. 1). The $6s5d\ ^3D_J$ states are metastable, with lifetimes greater than 1 sec [1,2]. Using noble gases as the buffer gas, quenching collisions prove to be negligible. Thus the main loss mechanism of $6s5d\ ^3D_J$ state atoms out of the detection region is diffusion. The initial spatial distribution of these trapped atoms reflects the spatial intensity distribution of the pump laser. By probing out of the $6s5d\ ^3D_J$ states at different spatial positions in the vapor, we can follow the diffusion of the metastable atoms through the buffer gas and construct spatial number density profiles at various times after the pump laser fires. From the spatial density profiles, the temperature- and pressure-dependent diffusion coefficients D are determined. Finally, from these diffusion coefficients, the thermally averaged diffusion cross sections σ_D are found. Conversely, the ground-state atom spatial distribution has a ''hole'' in it due to depletion by the pump laser pulse. By tuning our probe laser to the $6s^2\ ^1S_0 \rightarrow 6s6p\ ^3P_1^o$ transition, we can investigate the diffusion of ground-state atoms back into the depleted region in the same manner as described above for the metastable atom diffusion.

The results for $\sigma_D(6s5d\ ^3D_J)$ are compared to previous measurements [3,4]. However, to the best of our knowledge, measurements of $\sigma_D(6s^2\ ^1S_0)$ have not been made previously. Experimental measurement of these cross sections provides a test of theoretical barium–noble-gas molecular potential curves. Recently, calculated molecular potential curves for Ba($6s^2\ ^1S_0$)-He and Ba($6s5d\ ^3D_J$)-He have become available [5]. We use these to calculate theoretical collision cross sections in order to compare them to our experimental results. The agreement between the experimental and theoretical collision cross sections is very good.

The organization of this paper is as follows. Section II presents a model of the experimental ground and excited atom spatial density profiles based upon solution of the diffusion equation under the conditions of our experiment. The experimental methods are discussed in Sec. III, including a detailed presentation of the measurement of the time-dependent spatial density profiles with the pulsed-pump–cw-probe laser technique. Our results are presented and discussed in Sec. IV. In Sec. V we present calculated cross sections, based upon recent Ba-He potential curves [5], for ground and metastable barium atoms diffusing through helium. These theoretical results are compared with those ob-

---

[*] Present address: AT&T Microelectronics, 9333 S. John Young Parkway, Orlando, FL 32819.

[†] Present address: Department of Physics, Drew University, Madison, NJ 07940.

[‡] Present address: Lockheed Martin Management and Data Systems, Computer Service Engineering, Valley Forge, PA 19841.

1050-2947/96/54(1)/449(13)/$10.00

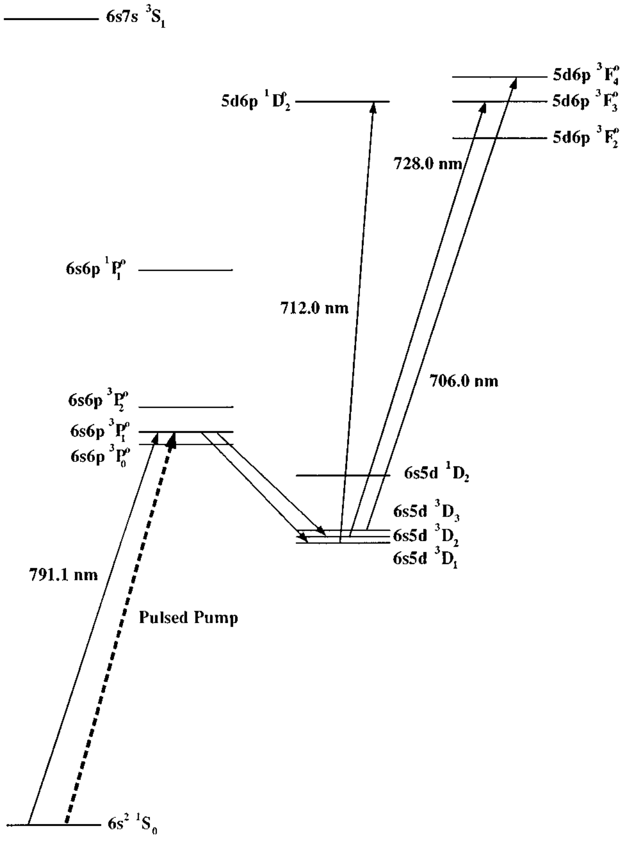

FIG. 1. Atomic barium energy-level diagram showing the levels involved in this work. The heavy dashed arrow indicates the transition pumped by the pulsed dye laser. The probe transitions (upward, solid arrows) are labeled with their respective wavelengths. The unlabeled, downward, solid arrows represent stimulated or spontaneous emission down to the $6s5d\ ^3D_{1,2}$ levels.

tained from the experiment. Conclusions are given in Sec. VI.

II. DIFFUSION MODEL

Since we operate with a barium density that is several orders of magnitude lower than the buffer gas density, we can ignore Ba-Ba collisions for the most part. In addition, the quenching and radiative rates out of the metastable manifold are assumed to be negligible over the time period of the measurements (this will be discussed in more detail in Sec. IV). Thus the diffusion of atoms through the heat-pipe oven is described by the diffusion equation

$$\frac{\partial n_i(\vec{r},t)}{\partial t} = D_i \nabla^2 n_i(\vec{r},t), \tag{1}$$

where D_i is the thermally averaged diffusion coefficient for atoms in state i and $n_i(\vec{r},t)$ is the number density of atoms in state i at position $\vec{r}$ and time t. There are several different ways to solve the diffusion equation, depending on the initial conditions and geometry (including boundary conditions), and these can be found in most upper-level textbooks on mathematical methods of physics [6]. Experimentally, we use a pulsed pump laser to create excited-state diffusing atoms. Thus our source of diffusing atoms approximates an infinite cylinder geometry with no angular dependence (i.e., we assume that the distribution depends only on the radial coordinate). We also assume that the walls of the heat-pipe oven are very far away; i.e., we can let the oven radius approach infinity in the theoretical treatment. Over the time frame of this experiment, only a very small fraction of the excited atoms diffuse to the walls, so this assumption is valid. Finally, we assume that the initial radial distribution of metastable atoms is well approximated by a Gaussian function. (Note that even if this is not the case, it can be shown that any initial distribution will eventually evolve into a Gaussian if wall effects can be neglected.) In Sec. IV we will show that the measured distributions are indeed well fit by Gaussians. With these assumptions, the solution to the diffusion equation is found to be

$$n_i(\vec{r},t) = \frac{N_{0,i}}{\pi L}\,\frac{1}{(R_p^2+4D_it)}\,\exp\!\left(-\frac{r^2}{R_p^2+4D_it}\right) + n_i^{\mathrm{eq}}. \tag{2}$$

Here L is the vapor column length, R_p^2 is a constant that defines the width of the initial metastable level distribution just after the pulsed laser fires, and $n_i^{\mathrm{eq}} = n_i(\vec{r},t=\infty)$ is the uniform equilibrium density of atoms in state i. (n_i^{eq} is equal to zero for the $6s5d\ ^3D_J$ levels and is equal to the equilibrium vapor density at temperature T for the ground state.) The solution is normalized over all space so that $N_{0,i}$ (where $N_{0,{}^1S} = -N_{0,{}^3D}$) is the total number of additional i state atoms (in excess of n_i^{eq}) created in the nonuniform distribution at $t=0$. From Eq. (2), we can see that the spatial dependence of the atoms will remain Gaussian at all times, with the square of the width given by $(R_p^2+4D_it)$. Thus with increasing time, the Gaussian width increases while the amplitude decreases. Figure 2 shows two examples of the spatial and temporal dependence of $n_i(\vec{r},t)$ using Eq. (2).

Diffusion is a process that depends on both the mean free path of the diffusing atoms traveling through the vapor (this is related to the pressure p of the buffer gas through which the atoms move) and the mean relative velocity of the colliding atoms (which depends on the temperature T of the vapor). Kinetic theory [7] predicts

$$D = \frac{3}{8}\left(\frac{\pi}{2\mu}\right)^{1/2} \frac{1}{\sigma_D}\,\frac{(kT)^{3/2}}{p}. \tag{3}$$

Here μ is the reduced mass of the atom-perturber system (in our case the barium–noble-gas system), k is Boltzmann's constant, and σ_D is a thermally averaged velocity-changing collision (momentum transfer) cross section. Thus the value of the measured diffusion coefficient D is dependent upon the temperature and buffer-gas pressure. Solving Eq. (3) for σ_D, we obtain

$$\sigma_D = \frac{3}{8}\left(\frac{\pi}{2\mu}\right)^{1/2} \frac{1}{D}\,\frac{(kT)^{3/2}}{p}. \tag{4}$$

Thus the diffusion cross section σ_D, which is related to the interatomic barium–noble-gas potentials [8], can be determined by measurements of the diffusion coefficient. Such measurements can serve as a test of theoretical potentials as they become available. (Recently, theoretical barium-helium

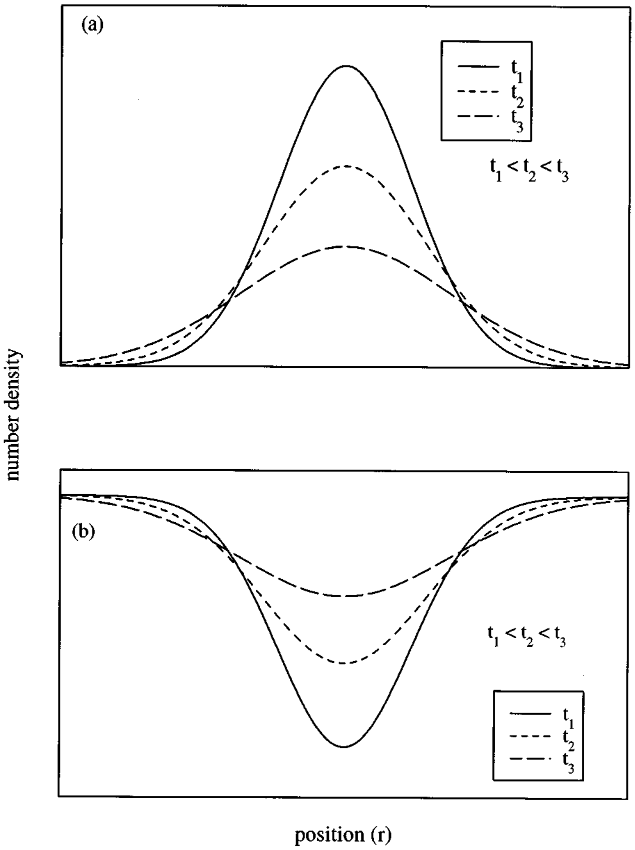

FIG. 2. Theoretical spatial dependence of the number density $n_i(r,t)$ at several different times [from Eq. (2)] for (a) metastable states and (b) the ground state.

potentials have been reported in the literature [5]. These are discussed in Sec. V and a comparison is made to our experimental results.)

We also report a standard diffusion coefficient D_0, which is related to D [using Eq. (3)] by

$$D_0 \equiv D\left(\frac{p}{p_0}\right)\left(\frac{T_0}{T}\right)^{3/2} = \frac{3}{8}\left(\frac{\pi}{2\mu}\right)^{1/2}\frac{1}{\sigma_D}\frac{(kT_0)^{3/2}}{p_0}. \tag{5}$$

Here T_0 and p_0 are standard conditions, taken to be $T_0=273$ K and $p_0=760$ Torr. Thus D_0 is nominally the diffusion coefficient at STP. The validity of Eq. (5) depends on the assumption that σ_D is independent of velocity, which may or may not be the case. (In Sec. V, we show that σ_D is not independent of velocity for the Ba-He case according to our calculations based on the potentials of Ref. [5].) We report D_0 for comparison purposes only and note that the experiments were done in a small range of temperatures. Therefore the important value reported here is σ_D which should only be considered valid for temperatures near 850 K.

III. EXPERIMENT

The experimental setup for the diffusion coefficient measurements, shown in Fig. 3, is almost identical to that used for the mixing and quenching measurements described in Ref. [9]. In the interest of brevity, the reader is referred to Ref. [9] for details. One notable addition, however, is that a mirror mounted on a translation stage was added to the setup.

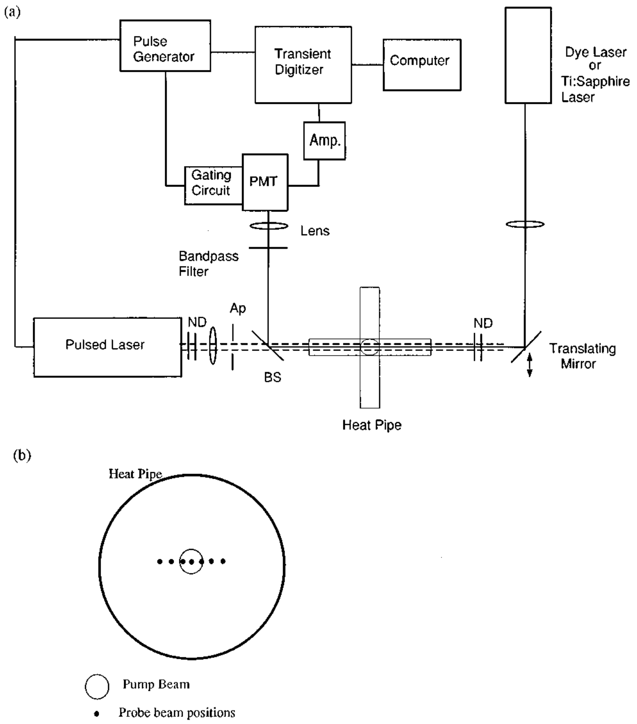

FIG. 3. (a) Experimental setup used for the diffusion experiments. PMT, photomultiplier tube; ND, neutral density filters; Ap, aperture; and BS, beam splitter. (b) Cross section of the heat-pipe oven showing the geometry of the pump and probe beams used to study the diffusion of the ground- and metastable-state barium atoms. This drawing is not to scale.

This allows the probe beam (counterpropagating with the pump beam) to be directed through the heat-pipe oven, with a (variable) parallel displacement between it and the pump [Fig. 3(b)]. This arrangement allows us to probe either the metastable- or ground-state densities both on and off axis and thus to measure their spatial distributions as a function of time following the pump pulse.

Barium is contained in a five-arm cross heat-pipe oven [10]. During the experiment, the heat-pipe oven was filled with a variable amount of one of the noble gases (helium, neon, argon, krypton, or xenon). For the diffusion of barium atoms through helium and argon, the noble gas was continuously flowed into, and pumped out of, the heat pipe so that impurities that baked off the oven walls would not accumulate. However, this procedure was not followed for neon, krypton, and xenon due to the cost of these gases. Instead a closed system was used in these cases. To prevent the accumulation of impurities, the closed system was prepared in the following manner (here neon will be used as an example). While the oven was heated, helium was flowed and pumped at a pressure of 3–4 Torr to protect the windows of the oven. During this time, impurities outgassing from the walls could be pumped out. The oven was heated using resistance heaters. Once the heat-pipe oven reached the operating temperature, the system was pumped down to about 0.5 Torr. Then about 25 Torr of neon was admitted and again the system was pumped down to about 0.5 Torr. Finally, neon was admitted to the system at the desired pressure and the system was closed to the pump. The closed system includes a capacitance manometer to monitor the pressure during the measurements. Three to seven different pressures were studied for each noble gas. For the closed system measurements, after each set the system was pumped down to about 0.5 Torr and fresh gas admitted to the system. Measurements were made starting with the highest pressure of interest and ending with the lowest. A set of measurements at a given noble-gas pressure took about half an hour and no systematic increase of the pressure was observed over that time period (i.e., any accumulation of impurities did not cause a measurable increase of the pressure inside the heat pipe oven). Because of the procedure used, these closed system measurements on neon, krypton, and xenon were always contaminated by some small admixture of helium. However, we believe that the procedure described above kept this contamination to a negligible level. Operating pressures ranged from 3 to 90 Torr, depending on the noble gas. The temperature was kept constant at a fixed value in the range 795–892 K during each set of measurements. These temperatures correspond to a barium vapor pressure of no more than a few mTorr. Thus the buffer-gas pressure was always much greater than the barium vapor pressure and the oven was not operating in the heat-pipe mode (i.e., the noble gas was thoroughly mixed with the barium).

Barium atoms were pumped into the $6s5d\ ^3D_J$ levels using a pulsed Nd:YAG (where YAG denotes yttrium aluminum garnet) laser (Quanta Ray, DCR11) pumped, dye laser (Lumonics HyperDYE-300) tuned to the $6s^2\ ^1S_0 \rightarrow 6s6p\ ^3P_1^o$ intercombination line at 791.3 nm. The power of the pump dye laser, before being reduced with neutral density filters, is typically about 50 mJ/pulse with a linewidth of about 0.3 cm^{-1} and a pulse duration of 6–8 nsec. While about 40% of the $6s6p\ ^3P_1^o$ atoms decay back to the ground state, the rest decay into the metastable manifold via the $6s6p\ ^3P_1^o \rightarrow 6s5d\ ^3D_{1,2}$ transitions [11–13]. Collisional mixing then transfers population among the $6s5d\ ^3D_J$ levels. This pumping scheme not only produced population in the $6s5d\ ^3D_J$ levels along the heat pipe axis, it also created a hole in the spatial distribution of ground-state atoms. Time-dependent densities within the three $6s5d\ ^3D_J$ levels or the ground state were then probed using a counterpropagating, weak, cw, laser. For the case of ground-state diffusion, we used a single-mode, cw, Ti:sapphire laser (Coherent 899-29), which could be tuned over the $6s^2\ ^1S_0 \rightarrow 6s6p\ ^3P_1^o$ transition. For the metastable-state diffusion, we used a single-mode, cw, ring dye laser (Coherent 699-29), which could be tuned into resonance with either the $6s5d\ ^3D_1 \rightarrow 5d6p\ ^1D_2^o$, the $6s5d\ ^3D_2 \rightarrow 5d6p\ ^3F_3^o$, or the $6s5d\ ^3D_3 \rightarrow 5d6p\ ^3F_4^o$ transition at 712.0, 728.0, or 706.0 nm, respectively. All three transitions out of the metastable levels were studied under identical conditions using argon buffer gas. The collisional mixing between the $6s5d\ ^3D_J$ levels couples the diffusion of atoms in these three levels [9]. Therefore, under these conditions, the separate diffusion coefficients cannot be measured. But instead we determine an average diffusion rate for $6s5d\ ^3D_J$ atoms. Results from the barium-argon metastable state measurements confirm that the same diffusion coefficient is obtained from all three probe transitions [14]. For helium, neon, krypton, and xenon only the $6s5d\ ^3D_2 \rightarrow 5d6p\ ^3F_3^o$ transition was probed.

The pump beam was typically apertured to a diameter of 1–3 mm and collimated through the heat-pipe oven using a 2-m focal length lens. The probe beam was attenuated to ~80 μW and apertured or focused to a diameter of ~0.5 mm. Two-dimensional charge coupled device (CCD) photodiode array (SpectraSource Instruments model LYNXX PC) images of the beam profile were recorded to ensure that the probe beam diameter remained constant over the length of the vapor. In addition, the pump beam energy was reduced to a few μJ/pulse for the metastable state measurements and to a few hundred μJ/pulse for the ground-state measurements to reduce saturation effects that would otherwise cause the initial population distribution to be non-Gaussian. [We found that using a pump beam that was too intense caused significant off-axis metastable production (relative to the on-axis population that is saturated), presumably due to the spatial tails of the pump laser Gaussian radial intensity distribution.] Note that the result of this pump laser attenuation was that the threshold for stimulated emission on the $6s6p\ ^3P_1^o \rightarrow 6s5d\ ^3D_{1,2}$ transitions was not always reached (in contrast to the mixing and quenching experiments reported in Refs. [9] and [14]). At the reduced pump energies used, we also found the initial population distribution to be well represented by a Gaussian. Also, under these pump conditions, the metastable level probe transitions were not optically thick at line center, so the frequency of the highly attenuated probe beam was tuned to line center of each transition of interest. On the other hand, the $6s^2\ ^1S_0 \rightarrow 6s6p\ ^3P_1^o$ transition remained optically thick at line center, even following the firing of the pulsed pump laser. Thus, for probing the Gaussian hole created in the ground-state spatial distribution, the probe laser was detuned from line center to a point where the attenuation was ~75–85 % before the pump laser fired. Due to depletion of the ground state, the transmission of the probe typically rose to ~50% on axis just after the firing of the pump laser.

The transmitted probe laser intensity was detected by a gated photomultiplier tube (Hamamatsu R2368; PMT in Fig. 3). The PMT was chosen for the spatial uniformity of its cathode response. The gating circuit turned on the PMT for up to 350 μsec, protecting it from overload from continuous probe laser illumination. The signal was recorded on a transient digitizer (Tektronix model 7912 HB or HD), which averaged data over 64 shots of the pulsed laser. The averaged signal from the digitizer was stored on a computer.

The time evolution of the spatial density profiles was mapped pointwise in the following manner. The probe laser was set to a specific spatial offset from the pump beam. Then, the time dependence of the probe beam absorption was obtained. Typical signals from the digitizer for both the ground state and the metastable state are shown in Fig. 4. Note that the digitizer and gating circuit are pretriggered so that data before the pulsed laser fires can be recorded (before the pulsed laser fires there is no population in the $6s5d\ ^3D_J$ levels and a uniform distribution $n_{^1S}^{\mathrm{eq}}$ in the ground state). These data (which we will refer to as "$t<0$ data" because we take $t=0$ as the time the pulsed laser fires) are used to normalize the data taken after the laser pulse. This normalization corrects for small changes in the cathode sensitivity with position and small drifts in the probe laser power or frequency. Measurements of the probe transmission vs time were repeated for many parallel displacements of the probe beam relative to the pump, over the diameter of the heat-pipe

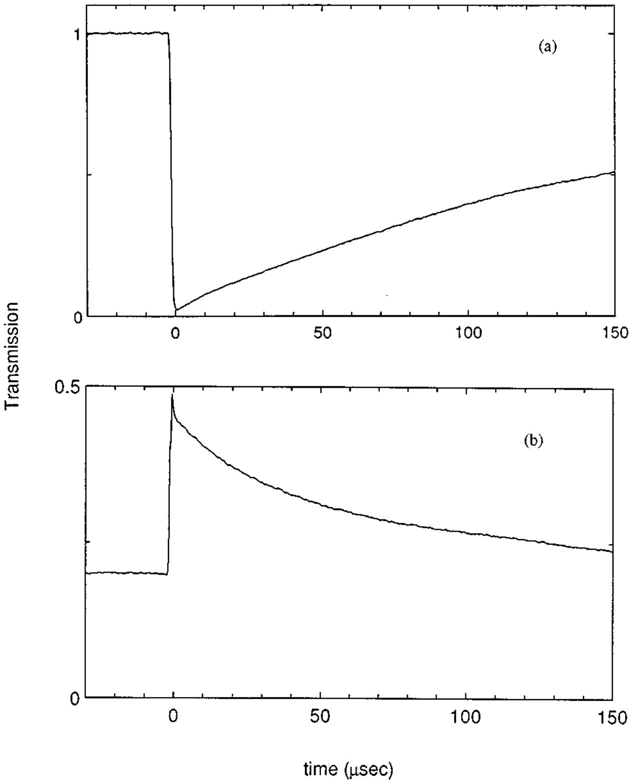

FIG. 4. On-axis ($r=0$) probe laser transmission $[\exp(-k_\nu L)]$ versus time when the probe laser was tuned to (a) the $6s5d\ ^3D_2 \rightarrow 5d6p\ ^3F_3^o$ transition and (b) the $6s^2\ ^1S_0 \rightarrow 6s6p\ ^3P_1^o$ transition. The oven temperature was 795 K and the argon pressure was 5 Torr for both measurements. Note that the pulsed pump laser fired at $t=0$. Zero transmission was obtained by blocking the probe beam. Note also that the probe laser beam was partially absorbed before the pump laser fired in the ground-state measurements. This is due to the equilibrium ground-state population. The average absorption coefficient measured during the time interval before the pulsed laser fires is $k_\nu(r,t<0)$ (see the text).

oven. The probe transmission was observed to change with time after the firing of the pump laser due to diffusion of the atoms and redistribution of population among the states. The step size for moving the probe beam was 0.318 ± 0.013 mm in all cases. The sequence of spatial offsets was chosen randomly, with the exception of the barium ($6s5d\ ^3D_J$) -argon diffusion measurement. The sequence of measurements of $6s5d\ ^3D_J$ atom diffusion through argon (which was the first set of measurements carried out) was made by systematically stepping the probe beam across the central region of the heat pipe from one extreme where the probe absorption was indistinguishable from zero to the other opposite extreme [14]. Since this procedure is subject to systematic errors due to pump laser drift, for which we must compensate, we switched to a random sequence of spatial offsets plus a scaling procedure for all other measurements. After probe transmission vs time traces at three or four random spatial positions were recorded, the probe laser was moved back to the center position to check for pump laser drift. If the drift was small, the pump laser was readjusted to maximize the metastable-state excitation and we continued with the measurements. If the drift was large ($\geqslant 10\%$), the pump laser was readjusted and that set of probe transmission trace measurements was repeated. At the end, each measurement was scaled using an interpolation between the ''before'' and ''after'' center measurements. These procedures all but eliminated systematic effects due to pump laser drift. Zero baseline traces with all lasers blocked were recorded periodically in all sets of measurements.

IV. RESULTS AND DISCUSSION

The digitized transmission vs time traces (Fig. 4) contain all information concerning the full temporal and spatial evolution of the number density in a particular level following the firing of the pump laser. At each position r, the normalized transmission vs time trace was converted to a time-dependent absorption coefficient $k_\nu(r,t)$ using

$$I(r,t)=I_0(r)\ \exp\left[-k_\nu(r,t)L\right]. \tag{6}$$

Here $I_0(r)$ is the incident probe beam intensity at position r and $I(r,t)$ is the time-dependent probe beam transmission through a length L of vapor, measured at time t after the pump laser fired. This expression can be solved for $k_\nu(r,t)L$. The same expression for values of $t<0$ yields the absorption coefficient $[k_\nu L]_{\text{eq}}$ associated with the equilibrium population in the probed level. Thus we find

$$\begin{aligned} k_\nu(r,t)L-[k_\nu L]_{\text{eq}} &= -\ln\left[\frac{I(r,t)}{I_0(r)}\right]+\ln\left[\frac{I(r,t<0)}{I_0(r)}\right] \\ &= \ln\left[\frac{I(r,t<0)}{I(r,t)}\right] \end{aligned} \tag{7}$$

Experimentally we determine $[k_\nu L]_{\text{eq}}$ as the average opacity recorded for times $t<0$; $[k_\nu L]_{\text{eq}}=k_\nu(r,t<0)L$. For the metastable level, $[k_\nu L]_{\text{eq}}$ is zero (because the equilibrium population in $6s5d\ ^3D_j$ is zero); however, this is not true for the ground-state measurement. $k_\nu(r,t)$ is proportional to the number density $n(r,t)$ at a particular spatial position r. Thus $[k_\nu(r,t)L-k_\nu(r,t<0)]L$ is proportional to $n_i(r,t)-n_i^{\text{eq}}$. We do not need to know this proportionality constant, because we obtain the diffusion coefficient from the widths of the $n_i(r,t)-n_i^{\text{eq}}$ curves [see Eq. (2)]. However, it could easily be obtained from our previous line-shape studies [15,16]. Relative values of $n_i(r,t)-n_i^{\text{eq}}$ are simply given by values of $\ln[I(r,t<0)/I(r,t)]$. Note also that we do not divide out the vapor length L, since we are interested in relative changes in the signal, and L is a constant. Dividing by L, which has a large uncertainty, would simply introduce additional uncertainty into our results.

Figures 5(a)–5(d) and 6(a)–6(d) show the spatial density profiles obtained by probing the $6s^2\ ^1S_0 \rightarrow 6s6p\ ^3P_1^o$ and $6s5d\ ^3D_2 \rightarrow 5d6p\ ^3F_3^o$ transitions, respectively, at different times after the firing of the pump laser and at different noble-gas pressures. The error bars in the data reflect the noise in the digitized signal.

In order to determine the diffusion coefficient D for the ground and metastable levels at each pressure and for each noble gas, a Levenberg-Marquardt method [17] was used to fit the experimental data to a Gaussian function of the form

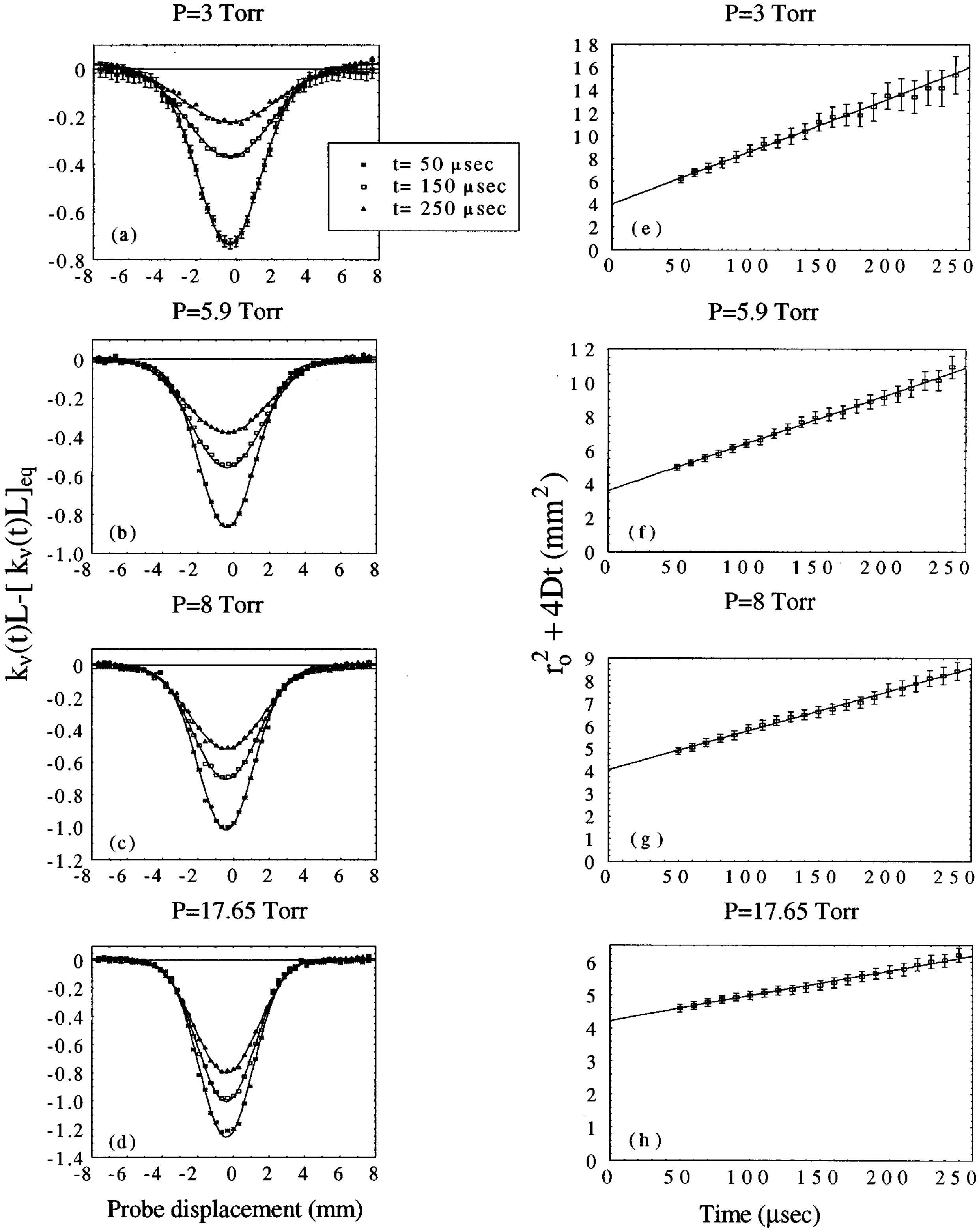

FIG. 5. (a)–(d) Ground-state $6s^2\ ^1S_0$ spatial density profiles, measured from absorption on the $6s^2\ ^1S_0 \rightarrow 6s6p\ ^3P_1^o$ transition at several different times (listed in the figure box) after the firing of the pulsed laser for Kr buffer-gas pressures of (a) 3, (b) 5.9, (c) 8, and (d) 17.65 Torr. The oven temperature was 866 K. The solid lines show the least-squares fits to Eq. (8). (e)–(h) Plots of the corresponding Gaussian width squared $r_0^2 + 4Dt$ vs time. Note that the vertical scales are not the same for the plots used to present data taken at different pressures.

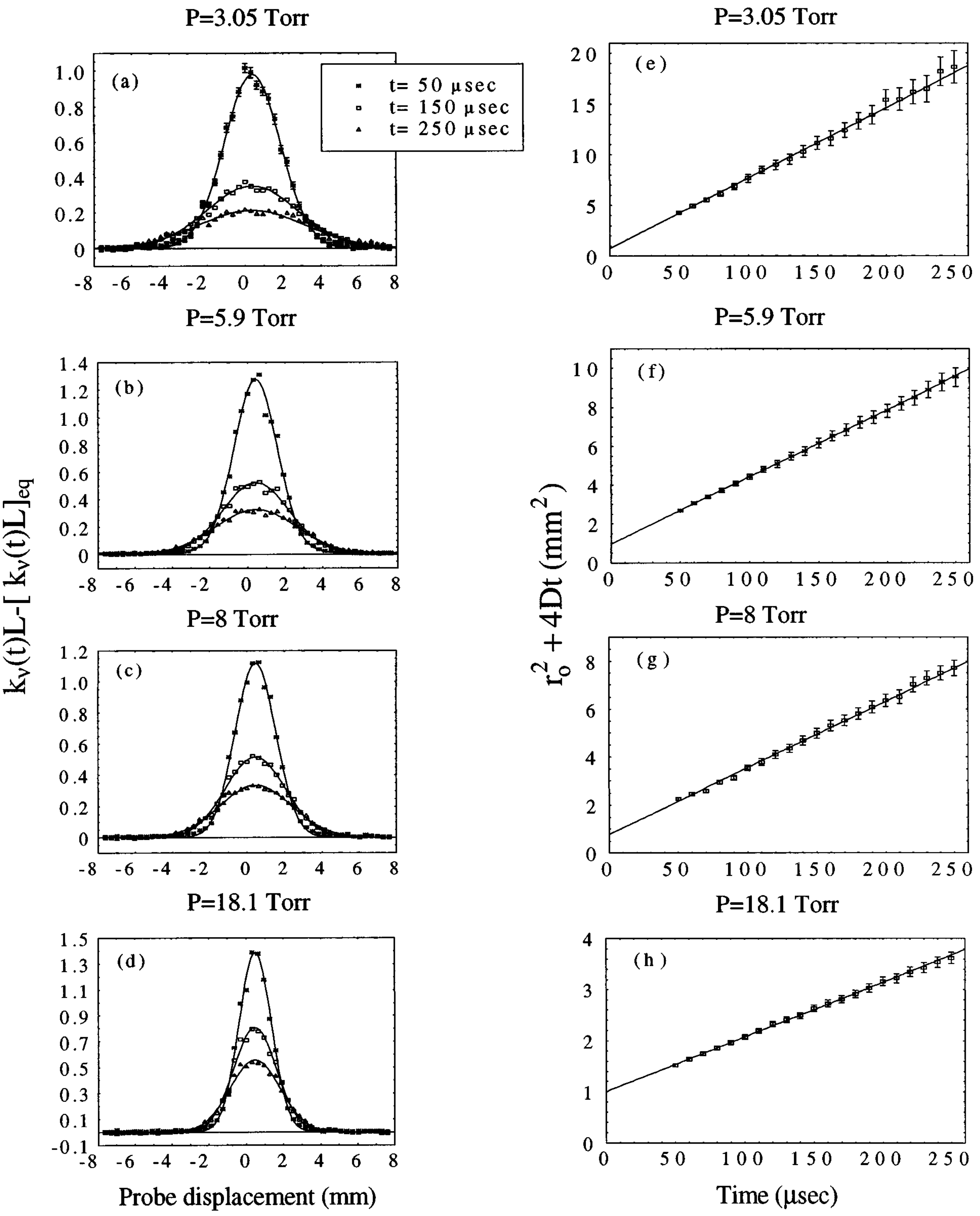

FIG. 6. (a)–(d) Metastable $6s5d\,^3D_2$ spatial density profiles, measured from absorption on the $6s5d\,^3D_2 \rightarrow 5d6p\,^3F_3^o$ transition at several different times (listed in the figure box) after the firing of the pulsed laser for Kr buffer-gas pressures of (a) 3.05, (b) 5.9, (c) 8, and (d) 18.1 Torr. The oven temperature was 864 K. The solid lines show the least-squares fits to Eq. (8). (e)–(h) Plots of the corresponding Gaussian width squared r_0^2+4Dt vs time. Note that the vertical scales are not the same for the plots used to present data taken at different pressures.

TABLE I. Pump and probe beam widths (R_p and r_p, respectively) and the initial width of the Gaussian spatial density profiles for the barium-krypton data. $r_0^{\text{calc}}=(R_p^2+r_p^2)^{1/2}$. r_0^{expt} is the $t=0$ intercept of the experimental width squared vs time curves.

Level probed	Pressure (Torr)	R_p (mm)	r_p (mm)	r_0^{calc} (mm)	r_0^{expt} (mm)
$6s^2\ {}^1S_0$	18.1	1.65	0.37	1.69	2.05
	8.0				2.01
	5.9				1.90
	4.0				1.98
	3.05				2.00
$6s5d\ {}^3D_J$	17.65	1.65	0.37	1.69	1.00
	8.0				1.03
	5.9				0.98
	3.0				0.87

$$n_i(r,t)-n_i^{\text{eq}} \propto \ln\left[\frac{I(r,t<0)}{I(r,t)}\right]=A\ \exp\left(\frac{(r-b)^2}{c}\right)+d \tag{8}$$

[see Eq. (2)]. Here A is the time-dependent amplitude and c is the Gaussian width squared. The offset parameter b allows us to account for any small mismatch of the pump and probe beam zero positions or shift of the distribution caused by a drift in the pump beam power and/or frequency. The parameter d allows for a nonzero base line, which can be due to noise in the signal and/or drift of the digitizer base line. With increasing time after the pulsed laser fires, the signal amplitudes decrease [see Figs. 5(a)–5(d) and 6(a)–6(d)]. A small error in the assumed base line (and therefore a small change in the fitted amplitude A) can lead to a large change in the fitted Gaussian width parameter c, especially when the Gaussian is short and wide as in the late time. Therefore for some sets this fitting parameter d was needed. (Note that the fitted base line d never fell outside of the experimental error bars of data points in the wings of the Gaussian spatial density profiles [see Figs. 5(a)–5(d) and 6(a)–6(d)].) In order to decide if the base line should or should not be a free parameter, the fitting was carried out both ways, and the reduced χ^2 of the Gaussian fits was used to determine which fit was preferable [18]. If a reduced $\chi^2 \geqslant 2$ occurred, the data were not used in calculating the diffusion coefficient.

Once the Gaussian fit was determined, the width squared c was plotted vs time [see Figs. 5(e)–5(h) and 6(e)–6(h)]. Our signal is determined by a convolution of the atom number density and the probe beam intensity. It can be shown that the measured signal is of the same form as Eq. (2), but with R_p^2 replaced with $r_0^2=r_p^2+R_p^2$, where R_p and r_p are the Gaussian widths of the pump and probe beams, respectively. Therefore, $c=r_0^2+4D_it$ [see Eq. (2)] and the temperature- and pressure-dependent diffusion coefficient D_i can be extracted from the slope of a straight-line fit of the data. The intercept of this plot is r_0^2, which is the measured width of the initial distribution (including effects of the probe beam spatial resolution) at $t=0$. r_p was determined from measurement of the probe laser beam spatial profile using the two-dimensional CCD array. R_p is taken to be the diameter of the aperture used to shape the (roughly collimated) pump beam. Note that diffraction tends to round the beam shape such that the net excitation is fairly well described spatially by a Gaussian function. Table I shows the experimental values for r_p and R_p as well as values of r_0 calculated from these values (r_0^{calc}). Table I also lists the square root of the intercepts of the plots shown in Figs. 5(e)–5(h) and 6(e)–6(h) (r_0^{expt}). r_0^{calc} falls between the values of $r_0^{\text{expt}}(6s^2\ {}^1S_0)$ and $r_0^{\text{expt}}(6s5d\ {}^3D_J)$. The differences between these values can be explained. Before the aperture, there is a 2-m focal length lens, gently focusing the pump beam to a point well past the heat pipe. Thus we expect a slight overestimation of r_0 based on the value calculated using the diameter of the aperture. This is in fact the case for $6s5d\ {}^3D_J$ measurements where the pump beam energy was on the order of μJ/pulse (small enough to avoid saturation effects). However, in order to have a substantial signal (against the nonzero background) in the ground-state diffusion measurements, the energy of the pump beam was increased by a factor of about 50 for those measurements. Saturation in the central region of the beam causes the excitation in the Gaussian wings of the beam to be similar to that on the beam axis, thus creating a wider excited atom spatial profile (or wider ground-state depletion region).

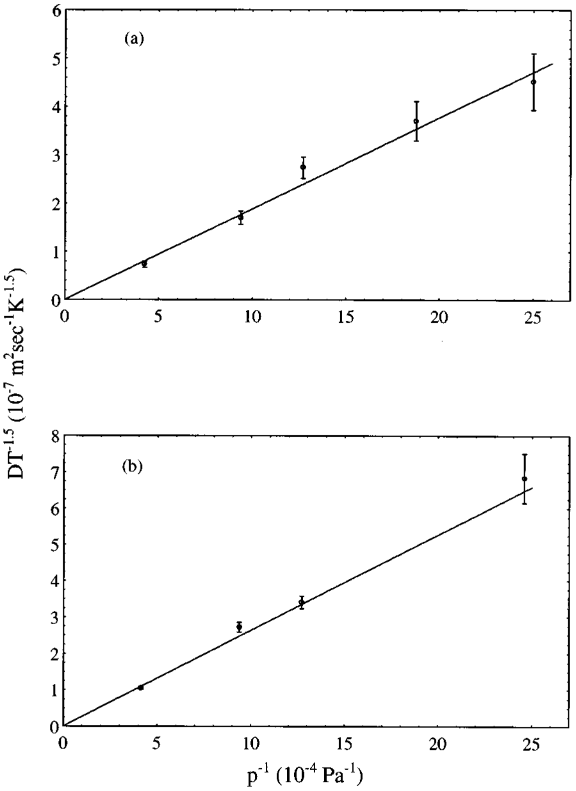

FIG. 7. Plots of $DT^{-1.5}$ vs p^{-1} for (a) ground-state and (b) metastable-state barium atoms diffusing through Kr at a temperature of about 865 K. σ_D and D_0 are determined from the slopes of the least-squares straight line fits [see Eqs. (3) and (5)].

Once D has been measured for all pressures and temperatures of interest, the diffusion cross section σ_D and standard diffusion coefficient D_0 can both be determined from the slope of the straight line obtained by plotting $DT^{-3/2}$ vs p^{-1} (see Fig. 7). Clearly, from Eq. (3) or (4), the slope of this line is given by $\frac{3}{8}\sqrt{\pi/2\mu}(k^{3/2}/\sigma_D)$. This can be inverted to yield the diffusion cross section, and D_0 can be obtained from Eq.

TABLE II. Experimental velocity-averaged cross sections σ_D and diffusion coefficients at STP D_0 for ground-state and metastable-state barium atoms diffusing through noble gases. The cross sections obtained in this work should be considered to be valid for the temperature range 795–892 K. Also presented for comparison are the previously measured values of σ_D and D_0 for diffusion of metastable $6s5d\ {}^3D_J$ atoms through the noble gases.

Noble gas	Temperature (K)	Pressure range (Torr)	D_0 (cm^2/sec)	σ_D (Å^2)
		Ground state		
helium	868[a]	20–90[a]	0.364 ±0.031[a]	36.7±3.1[a]
neon	871[a]	4–20[a]	0.181 ±0.019[a]	34.8±3.6[a]
argon	795[a]	5–50[a]	0.118 ±0.022[a]	40.2±7.6[a]
krypton	866[a]	3–18[a]	0.0839±0.0078[a]	43.5±4.1[a]
xenon	877[a]	3–22[a]	0.0593±0.0077[a]	54.2±7.0[a]
		Metastable states		
helium	886[a]	14–90[a]	0.466 ±0.045[a]	28.7±2.8[a]
	725–800[b]	10–500[b]	0.56 ±0.06[b]	25±3[b]
neon	867[a]	5–20[a]	0.259 ±0.019[a]	24.3±1.8[a]
	725–800[b]	10–500[b]	0.201 ±0.016[b]	32±3[b]
	750–900[c]		0.215 ±0.012[c]	29.3±1.6[c]
argon	800–873[a]	5–50[a]	0.139 ±0.010[a]	34.0±2.4[a]
	725–800[b]	10–500[b]	0.143 ±0.011[b]	34±3[b]
	750–900[c]		0.141 ±0.029[c]	33.5±6.9[c]
krypton	864[a]	3–18[a]	0.117 ±0.008[a]	31.1±2.1[a]
	750–900[c]		0.088 ±0.011[c]	42±5[c]
xenon	880[a]	3–21[a]	0.0783±0.0053[a]	41.1±2.8[a]
	725–800[b]	10–500[b]	0.084 ±0.008[b]	40±4[b]
	750–900[c]		0.073 ±0.008[c]	44.1±4.8[c]

[a] This work.

[b] Walker, Bonin, and Happer [3].

[c] Brust and Gallagher [4]. (Note that, in addition to the statistical error given above, the authors estimate a systematical error of 15% from the determination of the beam diameter in their experiment.)

(5). The error bars shown in Fig. 7 represent the statistical uncertainty from the fitted slopes of the width squared vs time curves, along with an estimated uncertainty of 0.02 Torr in the noble-gas pressure determination [9].

Our results are presented in Table II for both the metastable- and ground-state diffusion cross sections, along with error bars of ±7–19 %, which represent both statistical (~2–15 %) and systematic uncertainties. The latter includes a 3% systematic uncertainty in the temperature, which is measured by a thermocouple suspended in the vapor. In fact, the temperature is known to vary slightly along the length of the heat-pipe oven heated zone. Other systematic effects are discussed below. Our reported results are compared in Table II with the results of the previous metastable-state measurements of Walker, Bonin, and Happer [3] and of Brust and Gallagher [4]. We note that all the measurements of the metastable collision cross sections agree within error bars, except for the case of neon. It is also important to note that the error in the ground-state measurement is larger than the error in the metastable-state measurement. The increased error is due to the nonzero background ground-state population and the possible quenching of excited-state atoms during the time period of our measurements. The latter effect is discussed later in this section.

In our first set of measurements (metastable barium diffusing through argon), we observed that some data sets exhibited a slight drift of the entire metastable spatial profile from the center position as a function of time. We attributed this to a slow drift in the pump laser power and/or frequency. Since in these early measurements we scanned from one extreme of probe displacement (negative offsets) through zero displacement (overlapping beams) to the opposite maximum pump-probe separation, a systematic drop in the pump laser power or a drift of the laser away from the transition frequency would produce an apparent skewing of the initial distribution of the metastable-state densities. Numerical simulations showed that this effect would appear as an apparent drift of the centers of the fitted Gaussians with time. However, these simulations also showed that the error in the computed diffusion coefficient is less than 5% due to this effect, even for the unrealistically large drift assumed in the simulations. Thus these measurements of metastable barium diffusing through argon were not repeated. However, we switched to a random sequence of spatial positions plus a scaling procedure (described in Sec. II) for all subsequent measurements.

A second effect observed in the metastable-state, argon–buffer-gas measurements was the very long buildup times of the metastable level populations. Because we used low pump laser power in these experiments (to achieve a Gaussian

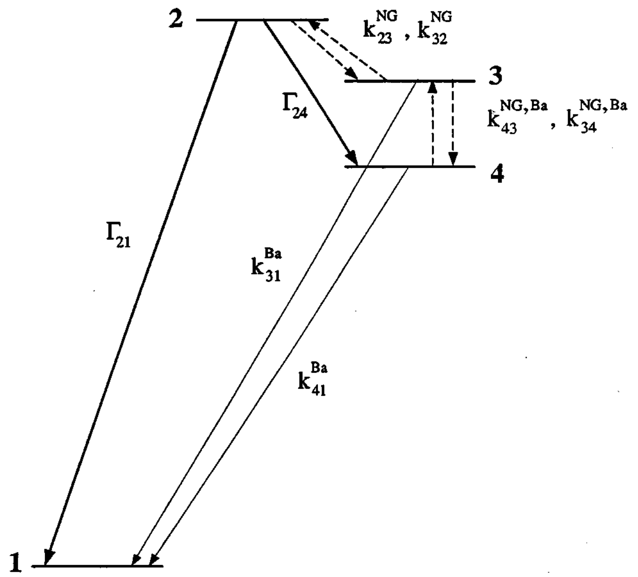

FIG. 8. Levels used in the four-level rate equation model with the nonzero population transfer mechanisms labeled. Values for the transfer rate coefficients are given in Table III. Here levels 1, 2, 3, and 4 represent the $6s^2\,{}^1S_0$, $6s6p\ {}^3P_1^o$, $6s5d\ {}^1D_2$, and $6s5d\ {}^3D_J$ levels of barium, respectively.

metastable level spatial distribution), the metastable levels were populated by spontaneous emission in this case. (Note that for other buffer gases, the metastable levels were populated by spontaneous emission, stimulated emission, or both). Thus the metastable-state densities take some time to build up. The natural lifetime of the $6s6p\ {}^3P_1^o$ level (which feeds the metastable levels) is about 1.2 μsec [4,11–13]. According to the results from Ref. [9], equilibrium within the $6s5d\ {}^3D_J$ manifold should be achieved (to within 90%) by argon–buffer-gas collisions in approximately 18 and 7 μsec, for pressures of 20 and 50 Torr, respectively. However, we observe the $6s5d\ {}^3D_J$ level populations are still building up after these times for these argon–buffer-gas pressures.

We systematically studied this question of density buildup by considering the total number of metastable atoms in the oven as a function of time, i.e.,

$$\int n(x,y,t)dx\ dy\ dz = 2\pi L \int n(r,t)r\ dr \equiv N(t), \qquad (9)$$

where L is the vapor column length and $N(t)$ is the total $6s5d\ {}^3D_J$ state density. Due to the rdr factor, the integral in Eq. (9) is not proportional to the area under the curves shown in Figs. 5(a)–5(d) and 6(a)–6(d), which represent a slice across the oven diameter. By calculating $N(t)$ for each set of profiles (using argon as a buffer gas), we found that the metastable-state buildup time for all three levels was greater than 10 μsec at the three pressures of interest and was longest at the lowest pressure. Metastable-state densities in all cases were found to stabilize to at least 90% of the final equilibrium value by 50 μsec after the pulsed laser fired.

Three sources of delayed population of the metastable levels suggest themselves. The first mechanism is radiation trapping on both the $6s6p\ {}^3P_1^o \rightarrow 6s^2\ {}^1S_0$ and $6s6p\ {}^3P_1^o \rightarrow 6s5d\ {}^3D_{1,2}$ transitions, which lengthens the effective lifetime of the $6s6p\ {}^3P_1^o$ level. The second possibility is excitation transfer within the $6s6p\ {}^3P_J^o$ manifold. This leads to population of the $6s6p\ {}^3P_0^o$ and $6s6p\ {}^3P_2^o$ levels, which are forbidden from radiating to the ground state. The third mechanism is collisional (Ba–noble-gas) transfer among the excited levels: $6s5d\ {}^3D_J 2w \leftrightarrow 6s5d\ {}^1D_2 \leftrightarrow 6s6p\ {}^3P_1^o$. Atoms transferred early on to the $6s5d\ {}^1D_2$ level can act as a delayed source of $6s6p\ {}^3P_1^o$ and $6s5d\ {}^3D_J$ atoms.

The radiation trapping explanation is consistent with the fact that lower buffer-gas pressures yield longer lifetimes [19]. This particular system presents a very interesting trapping problem (see Refs. [19–21] for more detailed discussions of radiation trapping). Since there is a large time-dependent population not only in the ground state but in the metastable levels as well, we can have trapping on all radiative channels out of the $6s6p\ {}^3P_1^o$ state. Right after the pump pulse, we have a central region of high metastable level population that is relatively depleted of ground-state atoms. Outside the pump beam most of the atoms are in the ground state. Both radiation trapping and atom diffusion cause these distributions to evolve in time. Thus, in different regions of the oven and at different times, the $6s6p\ {}^3P_1^o \rightarrow 6s^2\ {}^1S_0$ and $6s6p\ {}^3P_1^o \rightarrow 6s5d\ {}^3D_{1,2}$ photons are trapped by different amounts.

In order to study the second mechanism (collisional mixing among the $6s6p\ {}^3P_J^o$ levels), we directly probed the $6s6p\ {}^3P_{0,1,2}^o$ levels by monitoring the cw ring dye laser absorption when its frequency was tuned to the various $6s6p\ {}^3P_J^o \rightarrow 6s7s\ {}^3S_1$ transitions (see Fig. 1). In this experiment, we saw no evidence of population in either the ${}^3P_{0,2}^o$ levels (similar observations are reported in Refs. [4] and [22]), but the $6s6p\ {}^3P_1^o$ level exhibited decay times that were comparable to the metastable level buildup times we observed in the diffusion measurements. Thus it appears that collisional mixing from $6s6p\ {}^3P_1^o$ into $6s6p\ {}^3P_{0,2}^o$ is slow on this time scale.

The third mechanism, collisional transfer among the $6s6p\ {}^3P_1^o$, $6s5d\ {}^1D_2$, and $6s5d\ {}^3D_J$ levels, was studied using a four-level rate equation model. In this model, the levels $6s^2\ {}^1S_0$, $6s6p\ {}^3P_1^o$, $6s5d\ {}^1D_2$, and $6s5d\ {}^3D_J$ are labeled 1, 2, 3, and 4, respectively. The $6s5d\ {}^3D_J$ levels are treated as one level. In relation to the diffusion measurements, this is not a concern as long as the $6s5d\ {}^3D_J$ levels diffuse with comparable rates (i.e., if the diffusion cross sections of $6s5d\ {}^3D_1$, $6s5d\ {}^3D_2$, and $6s5d\ {}^3D_3$ are approximately equal and/or if the mixing within the $6s5d\ {}^3D_J$ manifold is rapid compared to diffusion and transfer out of the manifold) Figure 8 shows these model levels, with the relevant transfer mechanisms labeled, and Table III lists the values of all collisional and radiative rates used. The collisional transfer rate coefficients have been recently measured by Brust and Gallagher [4] and Vadla *et al.* [23]. The rate equations, valid after the pump laser pulse has terminated, are

$$\dot{n}_1 = (\Gamma_{21} + k_{21}^{\mathrm{Ba}} n_{\mathrm{Ba}}) n_2 + k_{31}^{\mathrm{Ba}} n_{\mathrm{BA}} n_3 + k_{41}^{\mathrm{Ba}} n_{\mathrm{Ba}} n_4, \qquad (10a)$$

TABLE III. Collisional rate coefficients and radiative rates used in the four-level rate equation modeling described in Sec. IV. In the model, we use $T=880$ K. Case (a): Total $6s5d\ ^1D_2$ and $6s5d\ ^3D_J$ depopulation rates due to Ba-Ba collisions are assumed to represent quenching to the ground state. Case (b): Total $6s5d\ ^1D_2$ and $6s5d\ ^3D_J$ depopulation rates due to Ba-Ba collisions are assumed to represent mixing of population between the $6s5d\ ^1D_2$ and $6s5d\ ^3D_J$ levels.

Barium–noble-gas collision rate coefficients [4] (10^{-12} cm^3/sec)

	helium	neon	argon	krypton	xenon
k_{23}^{NG}	77	40	43	22.9	5.9
k_{34}^{NG}	115	3.51	0.29	0.10	3.28

$k_{32}^{\mathrm{NG}}=0.0788k_{23}^{\mathrm{NG}}$

$k_{43}^{\mathrm{NG}}=0.0119k_{34}^{\mathrm{NG}}$

$k_{21}^{\mathrm{NG}}=k_{24}^{\mathrm{NG}}=k_{31}^{\mathrm{NG}}=k_{41}^{\mathrm{NG}}=k_{42}^{\mathrm{NG}}=0$

Barium-barium collision rate coefficients [23] (cm^3/sec)

Case (a)	Case (b)
$k_{21}^{\mathrm{Ba}}=k_{23}^{\mathrm{Ba}}=k_{24}^{\mathrm{Ba}}=k_{32}^{\mathrm{Ba}}=k_{34}^{\mathrm{Ba}}=k_{42}^{\mathrm{Ba}}=k_{43}^{\mathrm{Ba}}=0$	$k_{21}^{\mathrm{Ba}}=k_{23}^{\mathrm{Ba}}=k_{24}^{\mathrm{Ba}}=k_{31}^{\mathrm{Ba}}=k_{32}^{\mathrm{Ba}}=k_{41}^{\mathrm{Ba}}=k_{42}^{\mathrm{Ba}}=0$
$k_{31}^{\mathrm{Ba}}=5.1\times10^{-9}$	$k_{34}^{\mathrm{Ba}}=5.1\times10^{-9}$
$k_{41}^{\mathrm{Ba}}=5.1\times10^{-11}$	$k_{43}^{\mathrm{Ba}}=5.1\times10^{-11}$

Radiative rates [4] (sec^{-1})

$\Gamma_{21}=2.99\times10^5$

$\Gamma_{23}=0$

$\Gamma_{24}=4.41\times10^5$

$$\dot{n}_2=-(\Gamma_{21}+k_{21}^{\mathrm{Ba}}n_{\mathrm{Ba}}+\Gamma_{23}+k_{23}^{\mathrm{Ba}}n_{\mathrm{Ba}}+k_{23}^{\mathrm{NG}}n_{\mathrm{NG}}+\Gamma_{24}+k_{24}^{\mathrm{Ba}}n_{\mathrm{Ba}}+k_{24}^{\mathrm{NG}}n_{\mathrm{NG}})n_2+(k_{32}^{\mathrm{Ba}}n_{\mathrm{Ba}}+k_{32}^{\mathrm{NG}}n_{\mathrm{NG}})n_3+(k_{42}^{\mathrm{Ba}}n_{\mathrm{Ba}}+k_{42}^{\mathrm{NG}}n_{\mathrm{NG}})n_4, \tag{10b}$$

$$\dot{n}_3=(\Gamma_{23}+k_{23}^{\mathrm{Ba}}n_{\mathrm{Ba}}+k_{23}^{\mathrm{NG}}n_{\mathrm{NG}})n_2-(k_{31}^{\mathrm{Ba}}n_{\mathrm{Ba}}+k_{32}^{\mathrm{Ba}}n_{\mathrm{Ba}}+k_{32}^{\mathrm{NG}}n_{\mathrm{NG}}+k_{34}^{\mathrm{Ba}}n_{\mathrm{Ba}}+k_{34}^{\mathrm{NG}}n_{\mathrm{NG}})n_3+(k_{43}^{\mathrm{Ba}}n_{\mathrm{Ba}}+k_{43}^{\mathrm{NG}}n_{\mathrm{NG}})n_4, \tag{10c}$$

$$\dot{n}_4=(\Gamma_{24}+k_{24}^{\mathrm{Ba}}n_{\mathrm{Ba}}+k_{24}^{\mathrm{NG}}n_{\mathrm{NG}})n_2+(k_{34}^{\mathrm{Ba}}n_{\mathrm{Ba}}+k_{34}^{\mathrm{NG}}n_{\mathrm{NG}})n_3-(k_{41}^{\mathrm{Ba}}n_{\mathrm{Ba}}+k_{42}^{\mathrm{Ba}}n_{\mathrm{Ba}}+k_{42}^{\mathrm{NG}}n_{\mathrm{NG}}+k_{43}^{\mathrm{Ba}}n_{\mathrm{Ba}}+k_{43}^{\mathrm{NG}}n_{\mathrm{NG}})n_4. \tag{10d}$$

Here $n_{\mathrm{Ba}}=n_1+n_2+n_3+n_4$, Γ_{ij} is the radiative rate from level i to level j, and k_{ij}^{NG} and k_{ij}^{Ba} are the collisional rate coefficients for transfer of population from level i to level j due to Ba–noble-gas collisions and to Ba-Ba collisions, respectively. It is assumed that the primary effects of Ba-Ba collisions are quenching of excited atoms to the ground state; i.e., $\mathrm{Ba}(6s5d\ ^3D_J)+\mathrm{Ba}(6s^2\ ^1S_0)\rightarrow\mathrm{Ba}(6s^2\ ^1S_0)+\mathrm{Ba}(6s^2\ ^1S_0)$, excited-state–excited-state energy pooling collisions [24] and transfer of population between the $6s5d\ ^1D_2$ and $6s5d\ ^3D_J$ levels. The rate of transfer of population between the $^1D_2$ and ^3D_J levels due to collisions with ground-state barium atoms is generally comparable to or smaller than that due to collisions with noble-gas atoms [23] and these terms are directly included in the rate equations. On the other hand, we model the Ba-Ba quenching and energy pooling effects as a single depopulation rate out of each excited level, which is proportional to the total barium density. For consistency of the model, we assume that all such collisions populate the ground state, since levels above $6s6p\ ^3P_J^o$ are not considered. Quenching of $6s6p\ ^3P_J^o$, $6s5d\ ^1D_2$, and $6s5d\ ^3D_J$ atoms to the ground state in collisions with noble-gas atoms is known to be negligible [4,23]. A Runge-Kutta method was employed [17] to carry out the integration of the rate equations.

We considered in the model all buffer gases [He ($p=14$, 90 Torr), Ne ($p=3$, 20 Torr), Ar ($p=5$, 50 Torr), Kr ($p=3$, 20 Torr), and Xe ($p=3$, 25 Torr)] and two different sets of initial conditions: (i) all excited-state population starting in the $6s5d\ ^3D_J$ state (i.e., we assume that stimulated emission on the $6s6p\ ^3P_1^o\rightarrow6s5d\ ^3D_{1,2}$ transitions dumps all population to the lower states during the laser pulse) and (ii) all excited-state population starting in the $6s6p\ ^3P_1^o$ state. In both cases, the population in the ground state was taken to be 1.1×10^{13} cm^{-3}, similar to the experimental number density, and the excited-state population was taken to be 1×10^{10} cm^{-3}. For the case of argon buffer gas, $p=5$ Torr, our model shows a buildup time of close to 50 μsec; for argon, $p=50$ Torr, the buildup time is about 25 μsec (i.e., the buildup time is longer for lower pressures). Therefore the delayed population of the metastable levels observed experimentally with argon buffer gas could also be due to the collisional backtransfer mechanism. The model calculation results also show that in the worst cases (argon buffer gas, low pressure, and krypton buffer gas, all pressures) buildup of

TABLE IV. Thermally averaged diffusion cross sections for barium-helium collisions. The values are reported in units of Å^2. The theoretical values were calculated using the theoretical barium-helium interatomic potentials of Czuchaj *et al.* [5].

	Experiment (T=868,886 K)	Theory (T=880 K)	Theory (T=273 K)
$\sigma(6s^2\ ^1S_0)$	36.7±3.1	36.4	53.2
$\sigma(6s5d\ ^3D_J)$	28.7±2.8	26.2	45.4

population in the $6s5d\ ^3D_J$ states takes close to 50 μsec. Therefore, in the analysis, we did not use data recorded before $t=50$ μsec.

This model also answers another important question. In consideration of the collisional mixing among the $6s6p\ ^3P^o_1$, $6s5d\ ^1D_2$, and $6s5d\ ^3D_J$ levels, we must ask whether the measured metastable level diffusion cross section is actually some kind of average cross section for diffusion of $6s6p\ ^3P^o_1$, $6s5d\ ^1D_2$, and $6s5d\ ^3D_J$ level atoms. The model results show that, over the experimental time range of $t=50$–250 μsec, the total population of the $6s6p\ ^3P^o_1$ and $6s5d\ ^1D_2$ levels never exceeded 2% of the $6s5d\ ^3D_J$ population. Therefore, we believe that, to within the accuracy of the experiment, the measured quantity is $\sigma_D(6s5d\ ^3D_J)$ rather than an average over the $6s6p\ ^3P^o_1$, $6s5d\ ^1D_2$, and $6s5d\ ^3D_J$ levels.

From the results of Brust and Gallagher [4], Vadla *et al.* [23], and our rate equation modeling, we have found two possible channels for $6s5d\ ^3D_J$ atoms to ''quench'' to the ground state: Ba-Ba collisions [$\mathrm{Ba}(6s5d\ ^3D_J)+\mathrm{Ba}(6s^2\ ^1S_0)\rightarrow\mathrm{Ba}(6s^2\ ^1S_0)+\mathrm{Ba}(6s^2\ ^1S_0)$] and collisional backtransfer to $6s6p\ ^3P^o_1$ ($6s5d\ ^3D_J\rightarrow 6s5d\ ^1D_2\rightarrow 6s6p\ ^3P^o_1$) followed by radiative decay to the ground state. In either case, these atoms diffuse for some amount of time while in the $6s5d\ ^3D_J$ state before joining the ground-state distribution, which has been diffusing at a very different rate. This means that our measured value of the ground-state diffusion cross section is actually slightly contaminated by the excited-state diffusion:

$$\sigma_D^{\mathrm{meas}}(6s^2\ ^1S_0)=(1-Q)\sigma_D(6s^2\ ^1S_0)+Q\sigma_D(6s5d\ ^3D_J). \tag{11}$$

Q is derived in the following manner. According to our model calculations, the loss of atoms out of the $6s5d\ ^3D_J$ levels (which eventually end up in the ground state) can be described as an exponential decay

$$n_4(t_2)=n_4(t_1)\exp[-R_Q(t_2-t_1)], \tag{12}$$

where $n_4(t)$ is the population in the $6s5d\ ^3D_J$ levels at time t. R_Q is the net decay (quenching) rate. Since the observation time in the experiment, $(t_2-t_1)=200$ μsec, is small compared to $1/R_Q$, we can approximate the exponential as

$$\frac{n_4(t_2)}{n_4(t_1)}=\exp[-R_Q(t_2-t_1)]\approx 1-R_Q(t_2-t_1). \tag{13}$$

The fraction that is quenched in the interval (t_2-t_1) is therefore $R_Q(t_2-t_1)$. On average, these quenched atoms spend half their time diffusing while in the metastable states. Thus the weighing factor Q in Eq. (11) is $R_Q(t_2-t_1)/2=[n_4(t_1)-n_4(t_2)]/[2n_4(t_1)]$. The values of Q were determined from the four-level rate equation model in two limits based upon different assumptions for the rate coefficients. Vadla *et al.* [23] measured total depopulation cross sections for $\mathrm{Ba}(6s5d\ ^1D_2)$ and $\mathrm{Ba}(6s5d\ ^3D_J)$ due to collisions with ground-state barium atoms. The associated depopulation rate coefficients clearly provide upper limits for k_{31}^{Ba} and k_{41}^{Ba}. However, Vadla *et al.* state that these depopulation rates are probably dominated by mutual collisional mixing between $6s5d\ ^1D_2$ and $6s5d\ ^3D_J$. Thus we carried out the model calculations in two cases: (a) k_{31}^{Ba} and k_{41}^{Ba} are equal to the total depopulation rate coefficients of Ref. [23], while $k_{34}^{\mathrm{Ba}}=k_{43}^{\mathrm{Ba}}=0$, and (b) k_{34}^{Ba} and k_{43}^{Ba} equal the total depopulation rate coefficients of Ref. [23], while $k_{31}^{\mathrm{Ba}}=k_{41}^{\mathrm{Ba}}=0$. Case (a) gives the largest values for Q that fall in the range 0.06–0.13 for different gases at various pressures. Since we have measured the values of $\sigma(6s5d\ ^3D_J)$, we can, therefore, estimate the worst case errors in our measured ground-state diffusion cross sections by solving Eq. (11) for $\sigma_D(6s^2\ ^1S_0)$. These systematic corrections amount to less than 4%. In case (b), which is considered to be closer to the actual situation, the corrections are much smaller (<1%) and thus these effects were not included in the final ground-state cross sections reported in Table II. However, the reported error bars include the worst case error described above.

V. CALCULATED CROSS SECTIONS

The diffusion or momentum transfer cross sections can be calculated from theoretical Ba–noble-gas potentials [8]. Thus we have used the recent barium-helium potentials of Czuchaj *et al.* [5] to calculate both ground- and metastable-state diffusion cross sections. These calculations provide an interesting comparison with our experimental results, as well as providing a test of the quality of the theoretical curves.

For our calculations, we treat each electronic state of the Ba–noble-gas system separately. Then the standard partial-wave expansion [25] can be used to determine quantum-mechanical phase shifts and from them the appropriate cross sections. For each electronic state i and for several energies E, the set of phase shifts $\eta_l^i(E)$ was determined by solving the radial Schrödinger equation numerically using the logarithm derivative algorithm. The momentum transfer cross section σ_{MT}^i is defined in terms of the differential scattering cross section $d\sigma^i/d\theta$ as

$$\sigma_{\mathrm{MT}}^i=2\pi\int_0^\pi\frac{d\sigma^i}{d\theta}(1-\cos\theta)\sin\theta\,d\theta \tag{14}$$

and can be expressed in terms of the phase shifts as

$$\sigma_{\mathrm{MT}}^i=\frac{4\pi}{\kappa^2}\sum_l(l+1)\sin^2(\eta_{l+1}^i-\eta_l^i), \tag{15}$$

where $\kappa^2=2\mu E/\hbar^2$ and μ is the reduced mass. The thermally averaged diffusion cross section is defined [26–28] as

$$\overline{\sigma_D^i}=\frac{1}{2(kT)^3}\int_0^\infty E^2\sigma_{\mathrm{MT}}^i(E)\exp(-E/kT)dE. \tag{16}$$

$\overline{\sigma_D^l}$ was evaluated for $T=273$ and 880 K. The results are reported in Table IV, where they are compared with our experimental results. The agreement is quite good and confirms the fact that the ground-state diffusion cross section is indeed larger than the metastable-state cross section, in agreement with our experiment. $\overline{\sigma_D^l}$ ($T=273$ K) was calculated to test the validity of scaling the diffusion coefficient to standard temperature and pressure in order to report D_0. The results show that the collision cross section is dependent on the temperature of the vapor (or average collision energy) and therefore scaling the diffusion coefficient as in Eq. (5) is incorrect, at least for Ba-He. We report D_0 only for purposes of comparison to other published results, which are usually presented in this form.

VI. CONCLUSIONS

In conclusion, we have described a technique, using a narrow-band, cw probe laser and a pulsed pump laser, that can be used to map out the time evolution of the spatial number density profile in a heat-pipe oven for atoms in a specific atomic energy level. From these profiles, we have demonstrated that it is possible to determine the diffusion coefficient of the atoms in that particular state. In particular, we have determined the diffusion cross sections for metastable- and ground-state barium atoms moving through noble-gas perturber atoms. Our metastable-state diffusion cross sections are in good agreement with previously published results [3,4], while to the best of our knowledge, no previous experimental results for the ground-state diffusion cross sections have appeared in the literature. We have also been able to compare our experimental diffusion cross sections for barium-helium with results from theoretical barium-helium potentials [5]. These results agree very well with each other and support the quality of these theoretical potential curves, especially in the region of internuclear separations such that $E(R)-E(\infty)\sim kT$. We are confident that the experimental technique described here can be applied to other atom-perturber systems as a useful tool in studying the diffusion process.

ACKNOWLEDGMENTS

The authors are grateful to Dr. David Mugglin and Dr. Cedomil Vadla for useful discussions during the course of this work. We gratefully acknowledge financial support provided by the National Science Foundation (Grant No. PHY-9119498) and the U.S. Army Research Office (Grant No. DAAH04-93-G-0063). M.B. was supported through the National Science Foundation ''Research Experiences for Undergraduates'' program.

---

[1] I. I. Klimovskii, P. V. Minaev, and A. V. Morozov, Opt. Spektrosk. **50**, 847 (1981) [Opt. Spectrosc. (USSR) **50**, 464 (1981)].

[2] J. Migdalek and W. E. Baylis, Phys. Rev. A **42**, 6897 (1990).

[3] T. G. Walker, K. D. Bonin, and W. Happer, J. Chem. Phys. **87**, 660 (1987).

[4] J. Brust and A. C. Gallagher, Phys. Rev. A **52**, 2120 (1995).

[5] E. Czuchaj, F. Rebentrost, H. Stoll, and H. Preuss, Chem. Phys. **196**, 37 (1995).

[6] M. D. Greenberg, *Foundations of Applied Mathematics* (Prentice-Hall, Englewood Cliffs, NJ, 1978).

[7] R. D. Present, *Kinetic Theory of Gases* (McGraw-Hill, New York, 1958).

[8] T. P. Red'ko, Zh. Tekh. Fiz. **53**, 1730 (1983) [Sov. Phys. Tech. Phys. **28**, 1065 (1983)].

[9] E. Ehrlacher and J. Huennekens, Phys. Rev. A **50**, 4786 (1994).

[10] C. R. Vidal and J. Cooper, J. Appl. Phys. **40**, 3370 (1969).

[11] B. M. Miles and W. L. Wiese, At. Data **1**, 1 (1969).

[12] W. H. Parkinson and F. S. Tomkins, J. Opt. Soc. Am. **68**, 535 (1978).

[13] C. W. Bauschlicher, Jr., R. L. Jaffe, S. R. Langhoff, F. G. Mascarello, and H. Partridge, J. Phys. B **18**, 2147 (1983).

[14] E. Ehrlacher, Ph.D. thesis, Lehigh University, 1993 (unpublished).

[15] E. Ehrlacher and J. Huennekens, Phys. Rev. A **46**, 2642 (1992).

[16] E. Ehrlacher and J. Huennekens, Phys. Rev. A **47**, 3097 (1993).

[17] W. H. Press, S. A. Teukolsky, W. T. Vetterling, and B. P. Flannery, *Numerical Recipes in Fortran: The Art of Scientific Computing*, 2nd ed. (Cambridge University Press, New York, 1992).

[18] P. R. Bevington, *Data Reduction and Error Analysis for the Physical Sciences* (MGraw-Hill, New York, 1969).

[19] J. Huennekens, H. J. Park, T. Colbert, and S. C. McClain, Phys. Rev. A **35**, 2892 (1987).

[20] J. Huennekens and A. Gallagher, Phys. Rev. A **28**, 238 (1983).

[21] T. Colbert and J. Huennekens, Phys. Rev. A **41**, 6145 (1990).

[22] W. H. Breckenridge and C. N. Merrow, J. Chem. Phys. **88**, 2329 (1988).

[23] C. Vadla, K. Niemax, V. Horvatic, and R. Beuc, Z. Phys. D **34**, 171 (1995).

[24] J. A. Neuman, A. Gallagher, and J. Cooper, Phys. Rev. A **50**, 1292 (1994).

[25] N. F. Mott and H. S. W. Massey, *The Theory of Atomic Collisions* (Clarendon, Oxford, 1965).

[26] S. Chapman and T. G. Cowling, *The Mathematical Theory of Non-Uniform Gases*, 3rd ed. (Cambridge University Press, New York, 1970).

[27] W. A. Hamel, J. E. M. Haverkort, H. G. C. Werij, and J. P. Woerdman, J. Phys. B **19**, 4127 (1986).

[28] A. P. Hickman, D. T. Mugglin, and A. D. Streater, Opt. Commun. **102**, 281 (1993).